



Article

Using C-doped TiO₂ Nanoparticles as a Novel Sonosensitizer for Cancer Treatment

Chun-Chen Yang¹, Chong-Xuan Wang¹, Che-Yung Kuan^{2,3}, Chih-Ying Chi^{2,3},
Ching-Yun Chen^{3,4}, Yu-Ying Lin^{2,3}, Gin-Shin Chen³ , Chun-Han Hou^{5,*}
and Feng-Huei Lin^{3,6,*}

¹ Department of Materials Science and Engineering, National Taiwan University, Taipei 10617, Taiwan; d03527007@ntu.edu.tw (C.-C.Y.); r05527013@ntu.edu.tw (C.-X.W.)

² PhD Program in Tissue Engineering and Regenerative Medicine, National Chung Hsing University, Taichung 40227, Taiwan; 090115@nhri.edu.tw (C.-Y.K.); d103001707@mail.nchu.edu.tw (C.-Y.C.); 024016@nhri.edu.tw (Y.-Y.L.)

³ Institute of Biomedical Engineering and Nanomedicine, National Health Research Institutes, Miaoli County 35053, Taiwan; chingyun523@nhri.edu.tw (C.-Y.C.); gschen@nhri.edu.tw (G.-S.C.)

⁴ Department of Biomedical Sciences & Engineering, National Central University, Taoyuan City 32001, Taiwan

⁵ Department of Orthopedic Surgery, National Taiwan University, Taipei 10617, Taiwan

⁶ Institute of Biomedical Engineering, National Taiwan University, Taipei 10617, Taiwan

* Correspondence: chhou@ntu.edu.tw (C.-H.H.); double@ntu.edu.tw (F.-H.L.);
Tel.: +886-2-23123456#65274 (C.-H.H.); +886-2-27327474 (F.-H.L.)

Received: 18 August 2020; Accepted: 15 September 2020; Published: 17 September 2020



Abstract: Sonodynamic therapy is an effective treatment for eliminating tumor cells by irradiating sonosensitizer in a patient's body with higher penetration ultrasound and inducing the free radicals. Titanium dioxide has attracted the most attention due to its properties among many nanosensitizers. Hence, in this study, carbon doped titanium dioxide, one of inorganic materials, is applied to avoid the foregoing, and furthermore, carbon doped titanium dioxide is used to generate ROS under ultrasound irradiation to eliminate tumor cells. Spherical carbon doped titanium dioxide nanoparticles are synthesized by the sol-gel process. The forming of C-Ti-O bond may also induce defects in lattice which would be beneficial for the phenomenon of sonoluminescence to improve the effectiveness of sonodynamic therapy. By dint of DCFDA, WST-1, LDH and the Live/Dead test, carbon doped titanium dioxide nanoparticles are shown to be a biocompatible material which may induce ROS radicals to suppress the proliferation of 4T1 breast cancer cells under ultrasound treatment. From in vivo study, carbon doped titanium dioxide nanoparticles activated by ultrasound may inhibit the growth of the 4T1 tumor, and it showed a significant difference between sonodynamic therapy (SDT) and the other groups on the seventh day of the treatment.

Keywords: sonodynamic therapy; carbon doped titanium dioxide; sonosensitizers; ultrasound; cancer treatment; breast cancer treatment

1. Introduction

Cancer has been the leading cause of death in the US for 40 consecutive years. In 2019, there were 606,880 deaths from cancer projected to occur in the US [1]. Surgery, radiotherapy and chemotherapy are the most fundamental and effective cancer treatments. Nevertheless, it is hard to remove tumor cells comprehensively via surgery; radiotherapy and chemotherapy may not only kill the cancer cells but cause harm to healthy cells nearby and make patients feel fatigue. Immunotherapy is likely to interfere with the immune system and cause autoimmune disease. Hyperthermia is probably resisted by cancer cells after several heat treatments. Photodynamic therapy (PDT) is limited due to

the shallow penetration depth of light sources into tumor tissue. In previous studies, we used X-ray as an alternative light source which provided a novel therapeutic approach for deep-seated tumor/cancer treatment [2–4]; however, the annual radiation dose limit was another issue. Thus, an alternative therapy with fewer side effects was proposed by Umemura and Yumita, called “Sonodynamic therapy (SDT)” [5]. SDT can focus the ultrasound energy on the deeply located tumor site, which overcomes the shortcoming of PDT. SDT is considered to be a safer and more acceptable therapy for patients compared to radiotherapy and chemotherapy [6]. It is noninvasive, and the apparatus is relatively inexpensive [7,8].

SDT consists of three basic elements: ultrasound, sonosensitizer and oxygen molecules. The mechanism of SDT is that the nonthermal effect of acoustic cavitation generated by sonoluminescence, and the sonoluminescent light activates the sonosensitizer, leading to the electronic excitement of the sonosensitizer [7]. When the excited sonosensitizer decays back to the ground state, the released energy transfers to oxygen to generate the highly reactive singlet oxygen ($^1\text{O}_2$) [9]. Meanwhile, the energy may lead to pyrolysis reaction of the water near the exposed site of ultrasound and generate hydroxyl radicals ($\bullet\text{OH}$). These reactive oxygen species (ROS) may cause the death of the tumor cells afterwards [10]. ROS plays an important role in cellular signaling pathways, such as metabolism, growth, differentiation and death signaling, and react with molecules by reversible oxidative modifications. Excess generation of ROS may cause cell senescence and death to intracellular biomacromolecules, such as protein, lipid, RNA and DNA, via oxidative damage [11].

Ultrasound is a mechanical wave with periodic vibrations in a continuous medium at frequencies greater than 20 kHz [12]. Ultrasound is able to penetrate tissue with less attenuation of energy. Therefore, it can be applied to medical diagnosis and therapeutic use. For a medical diagnosis purpose, the ultrasound is irradiated at a frequency of 2.0 to 28.0 MHz with low-energy irradiation to prevent tissue from damaging. For therapeutic use, the ultrasound is irradiated at a frequency of 0.5 to 3.0 MHz with higher doses of energy to generate the desired biological results [13]. For SDT, low-intensity ultrasound is used to induce the non-thermal and sono-chemical effects to activate sonosensitizer to cause the damage and even the death of tumor cells [14]. The non-thermal effect of ultrasound in SDT is cavitation that involves formation, growth and collapse of cavitation bubbles [7]. Under ultrasound irradiation, the static pressure of the aqueous solution decreases below the vapor pressure, and water may evaporate into gas bubbles. The cavitation bubbles nucleate in the presence of impurities or pre-existing bubbles in solution and oscillate in the phase under irradiation [15]. During the ultrasound irradiation, bubbles grow increasingly larger and stop growing when the static pressure equals the vapor pressure. They may start to break down from its weakest spot when the static pressure exceeds the vapor pressure, and then collapse (known as inertial cavitation) led to a highly concentrated energy release [16,17]. The released energy leads to the pyrolysis reaction of the water, which generate ($\bullet\text{OH}$) and short light pulses (known as sonoluminescence) [18]. Sonoluminescence involves intense ultraviolet-visible light, which can excite sonosensitizer to generate ROS [19].

Sonosensitizers play a critical role in SDT that can enhance the effect of ultrasound. The development of sonosensitizers had grown swiftly in recent decades due to the known mechanisms of cell apoptosis for SDT [20]. The porphyrin-based sonosensitizers, such as photofrin, hematoporphyrin, 5-ALA (5-aminolevulinic acid) and chlorin-e6, are the most often used sonosensitizers in SDT research [7]. However, porphyrin-based sonosensitizers have phototoxicity on the skin that may affect both tumor cells and normal cells under a certain wavelength of light or energy irradiation in PDT studies, which means that this issue may also take place in SDT [20]. On the other hand, most sonosensitizers were hydrophobic and easy to aggregate in physiological condition, leading to a reduction in their ROS production [21]. Nonetheless, the development of nanoparticles shows a promising potential to solve these problems. Among many nanosensitizers, titanium dioxide (TiO_2) has attracted the most attention due to its properties [21]. TiO_2 is widely used in many territories based on low toxicity, high stability, high photocatalytic activity and low cost [22,23]. Compared to porphyrin-based sonosensitizers which are quickly degraded under oxidizing conditions, TiO_2 exhibits high stability because it is highly resistant to

degradation by ROS. TiO₂ exhibits three kinds of crystal structures, namely anatase, rutile and brookite. Anatase and rutile are the most common in the utilization of crystal structures, and brookite is less used in industrial application. Even though anatase ($E_g = 3.2$ eV) has a wider bandgap than rutile ($E_g = 3.0$ eV), anatase shows higher photoactivity due to its larger specific surface area that anatase is more suitable to be used as a photocatalyst [24]. In previous studies, the anatase structure of TiO₂ has been utilized as a sonocatalyst to generate ROS under ultrasound irradiation [10,14]. Nonetheless, the wide bandgap of anatase requires a greater energy to trigger. Carbon has previously been doped in the semiconductors to form a new valence band, thus narrowing the bandgap [25]. The addition of carbon may give TiO₂ an excess of conducting electrons or holes which is important for lowering the bandgap [23,24].

Hence, in this study, the sonosensitizer C-doped TiO₂ was synthesized through doping carbon into the anatase structure of TiO₂ to diminish the bandgap. A square wave of the ultrasound at a resonant frequency of 1.0 MHz, intensity of 0.33 MPa and duty cycle of 50% was used to induce the inertial cavitation and generate sonoluminescent light to activate the synthesized C-doped TiO₂.

2. Materials and Methods

2.1. Preparation of C-Doped TiO₂

C-doped TiO₂ was synthesized by the sol-gel method [23]. First, 2 g of Pluronic[®] F127 (Sigma-Aldrich, St. Louis, MO, USA) was dissolved in 40 mL 95% ethanol completely with vigorous stirring. Then, 5 mL titanium(IV) isopropoxide (TIP, Ti(OCH(CH₃)₂)₄, purity > 97%, Sigma-Aldrich) was added into the solution with magnetic stirring of 600 rpm. An amount of 3 g of D-(+)-glucose (C₆H₁₂O₆, Sigma-Aldrich), which was used as the carbon source, was dissolved in 6 mL ddH₂O. Then, the glucose solution was dropped into the TIP/Pluronic[®] F127 solution. The mixed solution was kept vigorously stirring at room temperature for 30 min. The precipitate was collected by centrifugation at 5000 rpm and washed with 95% ethanol for three times. The precipitate was then calcined at 400 °C for 2 h to obtain particles.

2.2. Material Characterization

The crystal structure of the synthesized C-doped TiO₂ was determined by X-ray diffraction (XRD; Rigaku TTRAX 3) with Cu K α radiation at a speed of 2° per minute at 40 kV and 30 mA from 20° to 60°. The surface morphology and particle size of C-doped TiO₂ were characterized by a scanning electron microscope (SEM; Nova Nano SEM 450). The structure and diffraction pattern of the material were analyzed by a transmission electron microscope (TEM; JEOL 2010F). The particle size of the material was reconfirmed via Zetasizer (Malvern Nano ZS). The chemical composition of the material was analyzed by an energy dispersive spectrometer (EDS; Nova Nano SEM 450) SEM attachment. To confirm that carbon had been doped in titanium dioxide and formed the bonding, C-doped TiO₂ was measured by auger electron spectroscopy (AES; JEOL JAMP 9510F) and X-ray photoelectron spectroscopy (XPS; Theta Probe).

2.3. Ultrasound Apparatus

Ultrasound irradiation was conducted with a function generator (Agilent 33521A) at a resonant frequency of 1.0 MHz and a duty cycle of 50% and amplified by a power amplifier (E&I 1040L) to generate a square wave with a negative pressure of 0.33 MPa and intensity of 1.8 W/cm² for 90 s in the whole experiment. Figure 1 shows the entire apparatus.

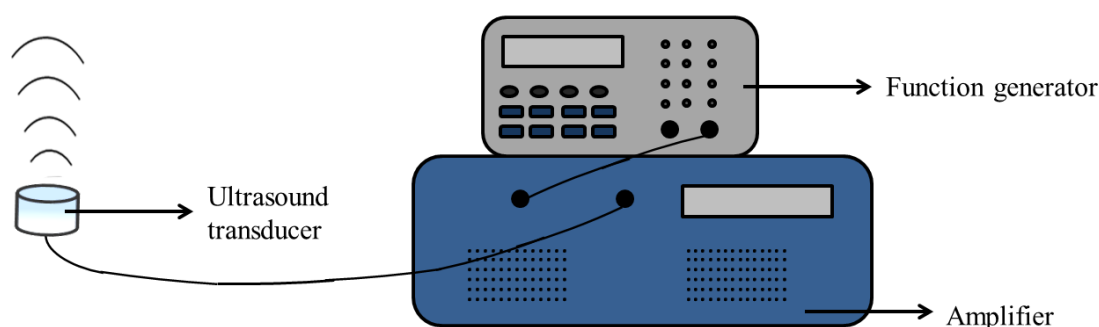


Figure 1. Ultrasound apparatus. The ultrasound transducer with a diameter of 2.0 cm was fixed with aluminum block by a rubber band to keep the transducer facing upward in the degassed water tank.

2.4. Preparation of Terephthalic Acid Solution and Evaluation of Ultrasound Parameter

First, 2 mM terephthalic acid (TA; Sigma-Aldrich) was dissolved in 800 mL ddH₂O. During ultrasound treatment, the experiments should be carried out under alkaline condition. Hence, 5 mL 1 M of NaOH was added in the solution. TA solution was stirred for 1 h under 4 °C and dark conditions to avoid photochemical reaction [26].

The experiment was divided into two groups. No US group was named as the control group: the US group was the group irradiated by ultrasound. The fluorescence signal intensity was measured by a multi-label plate reader with excitation and emission wavelengths at 310 and 420 nm, respectively.

2.5. Cell Culture and Animal Model

Briefly, L929 cells obtained from National Health Research Institutes were cultured in MEM medium (Minimum Essential Media, Sigma-Aldrich) with 10% Fetal bovine serum (FBS, Gibco) and 1% Antibiotic-Antimycotic (Gibco) and maintained in a 5% CO₂ atmosphere at 37 °C.

Breast cancer 4T1 cells obtained from National Health Research Institutes were used as model cancer cells in this study. The 4T1 cells were cultured in RPMI medium (RPMI-1640 Media (Sigma-Aldrich) with 10% Fetal bovine serum (FBS, Gibco) and 1% Antibiotic-Antimycotic (Gibco) and maintained in 5% CO₂ atmosphere at 37 °C.

6-week-old male BALB/c nude mice were used as a xenograft animal model in this study. The nude mice were injected subcutaneously with 2×10^6 4T1 cells suspended in 200 µL 1X PBS into the right thigh. All the animal experiments were approved by National Health Research Institutes (NHRI-IACUC-107013).

2.6. Evaluation of Biocompatibility for the Synthesized C-Doped TiO₂

The evaluation of biocompatibility in this study was based on International Standard ISO 10993. The cell viability induced by the synthesized C-doped TiO₂ was determined by the WST-1 test (TAKARA). L929 cells were seeded on a 96-well cell culture plate with a cell density of 10⁴ cells per well and incubated in 5% CO₂ atmosphere at 37 °C. Briefly, 0.2 g/mL of the materials was immersed in MEM medium for 16 to 24 h in 5% CO₂ atmosphere at 37 °C as material extracts. The control group included L929 cells without treatment. Zinc diethyldithiocarbamate (ZDEC, Sigma-Aldrich) and aluminum oxide (Sigma-Aldrich) were indicated as the “Positive Control” and “Negative Control” group, respectively. The C-doped TiO₂ group included cells cultured with C-doped TiO₂. After one-day incubation, the previous solution in each well was removed, and 100 µL of the supernatant of the material extracts was added into each well. After one-day incubation, the previous solution in each well was removed, and 100 µL fresh MEM medium with 10% WST-1 reagent was added. After 2 h incubation in 5% CO₂ atmosphere at 37 °C kept in the dark, the solution in each well was collected to measure absorbance at 490 nm by a microplate reader.

2.7. Detection of Cellular ROS Generation

ROS generation induced by the synthesized C-doped TiO₂ in SDT was measured by a DCFDA-cellular ROS detection assay kit (abcam). 4T1 breast cancer cells were seeded on 12-well cell culture plates with a cell density of 6×10^4 cells per well and incubated in 5% CO₂ atmosphere at 37 °C. After one-day incubation, the previous solution in each well was removed, and 1 mL 15 mg/mL synthesized C-doped TiO₂ in RPMI medium was added into each well. After 6 h incubation, ultrasound was then irradiated from the bottom of the cell culture plates in degassed water. The distance between ultrasound transducer and the bottom of the cell culture plate was around 5 mm. After US treatment, the cell culture plates were incubated for 2 h. The previous solution in each well was then removed and washed once with 1× PBS. An amount of 1 mL 20 μM 2',7'-dichlorofluorescein diacetate (DCFDA, abcam) in 1× buffer was added into each well for 30 min in 5% CO₂ atmosphere at 37 °C in the dark. The previous solution in each well was removed, and cells were washed with 1× PBS once. An amount of 1 mL 1× PBS was added into each well. The fluorescence signal intensity was measured by a multilabel plate reader with excitation and emission wavelengths at 485 and 535 nm, respectively [27]. The control group included 4T1 cells without treatment. The C-doped TiO₂ group included cells cultured with C-doped TiO₂. The US group included cells subjected to ultrasound irradiation. The SDT group included cells cultured with C-doped TiO₂ and subjected to ultrasound irradiation.

2.8. Evaluation of the Synthesized C-Doped TiO₂ in SDT In Vitro

WST-1 and LDH tests were used to evaluate the cell viability and cytotoxicity of the synthesized C-doped TiO₂ in SDT. In vitro, 6×10^4 4T1 cells suspended in 1 mL RPMI medium were seeded on 12-well cell culture plates and incubated in 5% CO₂ atmosphere at 37 °C. After one-day incubation, the previous solution in each well was removed, and 1 mL 15 mg/mL synthesized C-doped TiO₂ in RPMI medium was added into each well. After 6 h incubation, ultrasound was then irradiated from the bottom of the cell culture plates in degassed water. The distance between the ultrasound transducer and the bottom of the cell culture plate was around 5 mm. After ultrasound treatment, the cell culture plates were incubated for one day. For the WST-1 test, the previous solution in each well was removed, and 400 μL fresh RPMI medium with 10% WST-1 reagent was added. After 1 h incubation in 5% CO₂ atmosphere at 37 °C kept in the dark, the solution in each well was collected to measure absorbance at 490 nm by an Elisa reader. The control group included 4T1 cells without treatment. Zinc diethyldithiocarbamate (ZDEC) and aluminum oxide were indicated as the "Positive Control" and "Negative Control" group, respectively. The C-doped TiO₂ group included cells cultured with C-doped TiO₂. The US group included cells subjected to ultrasound irradiation. The SDT group included cells cultured with C-doped TiO₂ and subjected to ultrasound irradiation.

For the LDH test, 50 μL lysis solution was then added into each well of the Lysis group and then incubated in 5% CO₂ atmosphere at 37 °C for 30 min. Fifty μL of supernatant from each well was then transferred to a 96-well cell culture plate, and 50 μL LDH reagent was added into each well. After 15 min of reaction at room temperature in the dark, the cytotoxicity was measured by a microplate reader with absorbance at 490 nm. The C-doped TiO₂ group included cells cultured with C-doped TiO₂. The US group included cells subjected to ultrasound irradiation. The SDT group included cells cultured with C-doped TiO₂ and subjected to ultrasound irradiation.

2.9. Evaluation of SDT in In Vivo Tumor Growth

There were 4 different treatments exerted on nude mice: (1) the control group was injected with 200 μL 1× PBS at day 0 and day 7 without ultrasound irradiation; (2) the C-doped TiO₂ group was injected with 200 μL synthesized C-doped TiO₂ (150 mg/mL) in 1× PBS at day 0 and day 7 without ultrasound irradiation; (3) the US group was injected with 200 μL of 1× PBS at day 0 and day 7 with US irradiation; (4) the SDT group was injected with 200 μL synthesized C-doped TiO₂ (150 mg/mL) in 1× PBS at day 0 and day 7 with US irradiation. There were 5 nude mice in each group.

The tumor volume was measured by an electronic slide caliper using Equation (1), where L is the longest dimension and W is the shortest dimension, parallel to the mouse body [28].

$$V = 0.5 \times L \times W^2 \quad (1)$$

2.10. Histopathology

During sacrifice, cardiac puncture was used to obtain the blood samples. The samples were collected into tubes with 7.5% EDTA solution. Tumor and internal organs, including heart, liver, spleen, lung and kidney were also harvested and then fixed with 4% formaldehyde. These organs were embedded into the paraffin and further stained with hematoxylin and eosin (H&E) for histologic examination.

2.11. Statistics

All data are indicated as the mean \pm standard deviation. Statistical analysis was performed using one-way ANOVA followed by multiple comparisons with the Dunnett test, and the difference between the groups was deemed to be statistically significant when $p < 0.05$.

3. Results

The XRD pattern of the synthesized C-doped TiO₂ is shown in Figure 2a. It is indicated that the 2θ at 25.2°, 38.3°, 48°, 54.3° and 55.1° corresponded to the crystal form of (101), (004), (200), (105) and (211), which was completely matched with the standard pattern of the anatase structure of TiO₂ (JCPDS Card No. 21-1272). The surface morphology of C-doped TiO₂ was characterized by SEM as shown in Figure 2b,c. Figure 2d shows the chemical composition of the material analyzed by EDS, Ti, O and C elements with an atomic percent (At%) of 62.8, 32.8 and 4.4, respectively. The particles were spherical with a rough surface. The structure and diffraction pattern of the material were examined by TEM as shown in Figure 2e,f, respectively. C-doped TiO₂ formed in the aggregation of nanograins, and its particle size was in the range of 100 to 200 nm. The selected area diffraction pattern (SADP) of C-doped TiO₂ showed a ring pattern with the concentric rings from interior to outside, representing the crystal planes of (101), (004) and (105) which corresponded to the anatase phase. The particle size was precisely measured by Zetasizer as shown in Figure 2g. The precise particle size was 156.9 nm with a polydispersity index (PDI) of 0.137, which was in agreement with the analysis of SEM particle size (148.9 ± 26.3 nm) as shown in Figure 2h. Figure 3a shows the detection of chemical composition of the material by AES. In addition to the peaks related to Ti and O, C was detected at the energy of 263 eV. Figure 3b shows the XPS spectra of C-doped TiO₂ was at a binding energy of 282, 462 and 562 eV, representing O 1s, Ti 2p and C 1s, respectively. Figure 3c shows the XPS spectra of the C 1s scan: the peak of TiC was detected at binding energy around 282 eV [29]. Figure 3d shows the XPS spectra of the Ti 2p scan, the peak of Ti⁴⁺ was detected at a binding energy of 462 (Ti 2p_{1/2}) and 456 eV (Ti 2p_{3/2}). Figure 3e shows the XPS spectra of the O 1s scan: the peak of (Ti⁴⁺/Ti³⁺)-O was detected at a binding energy of 527 eV.

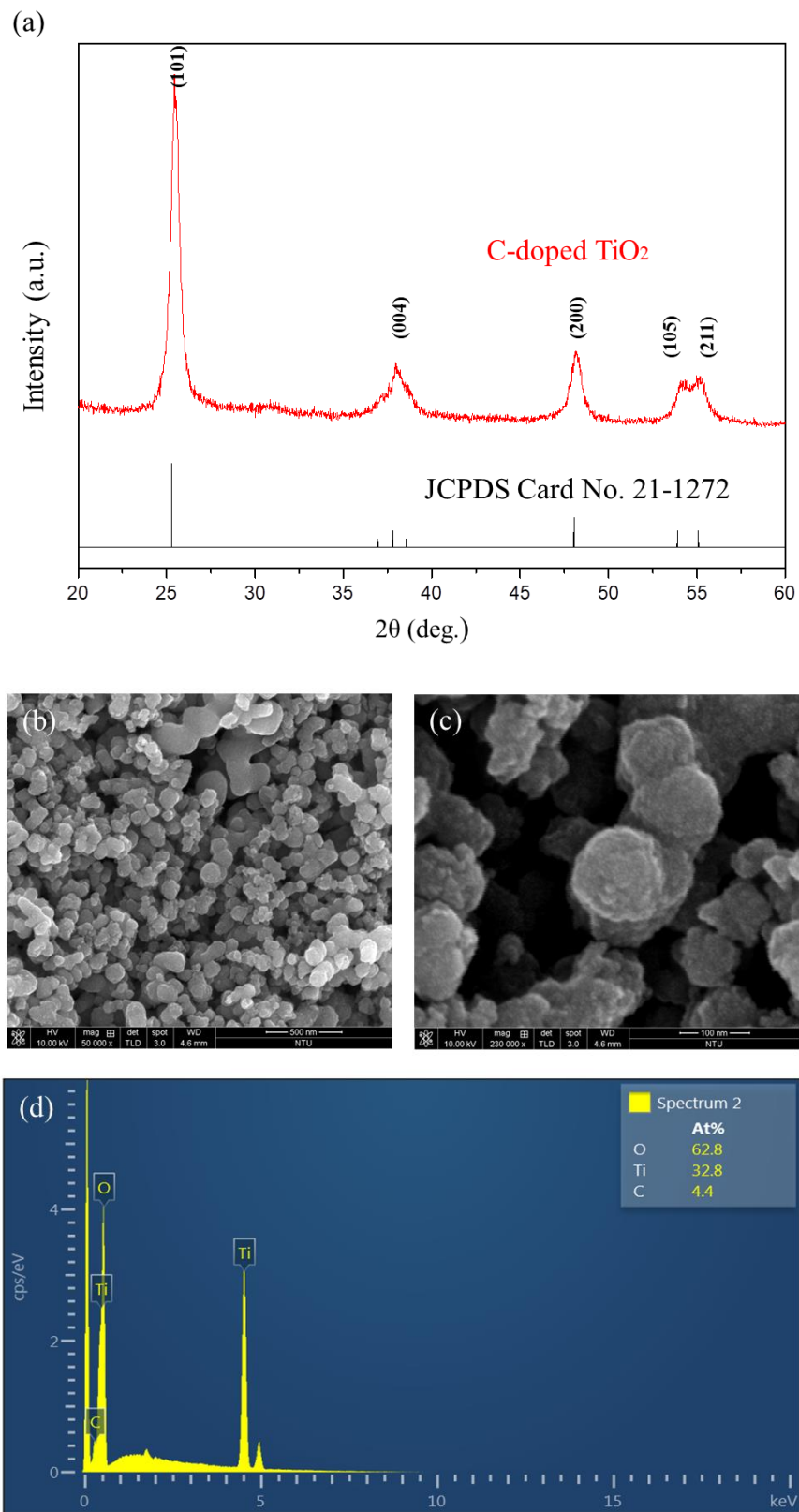


Figure 2. Cont.

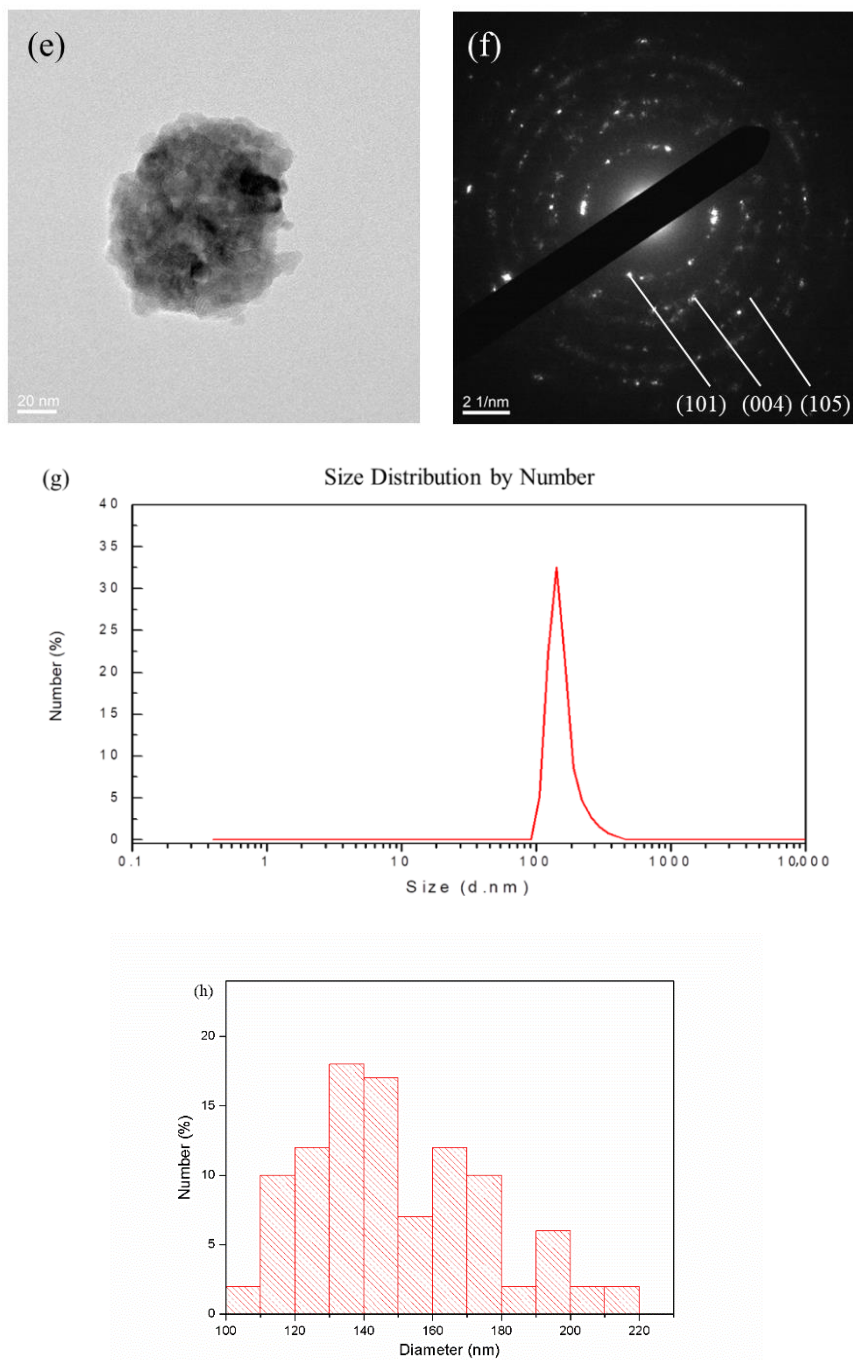


Figure 2. (a) XRD pattern of C-doped TiO₂, (b) low-magnification SEM images of C-doped TiO₂, (c) high-magnification SEM images of C-doped TiO₂, (d) EDS of C-doped TiO₂, (e) TEM images of C-doped TiO₂, (f) Diffraction pattern of C-doped TiO₂, (g) Size distribution of C-doped TiO₂ and (h) SEM particle size distribution of C-doped TiO₂.

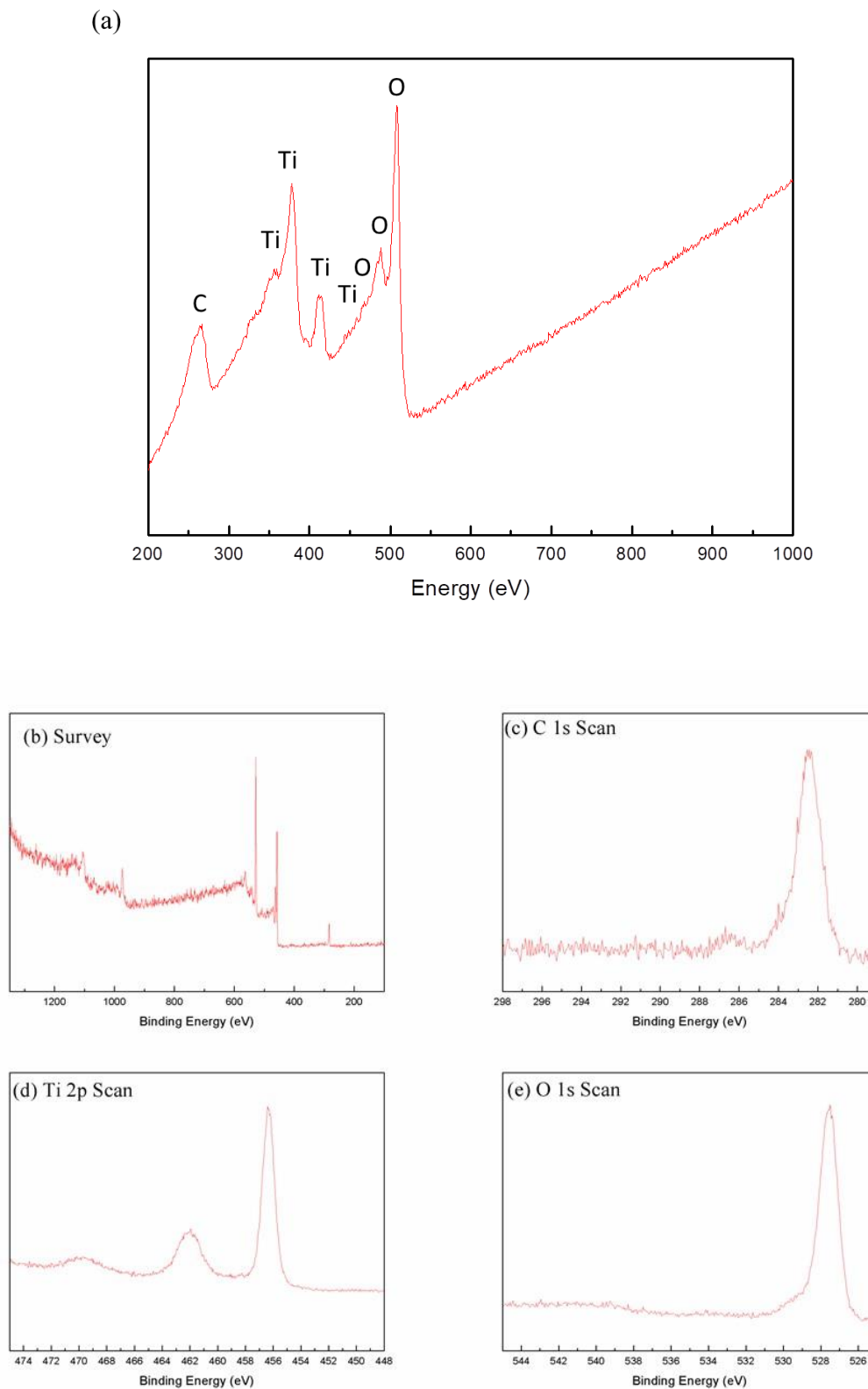


Figure 3. (a) AES spectra of C-doped TiO₂, (b) XPS spectra of C-doped TiO₂, (c) C 1s scan, (d) Ti 2p scan and (e) O 1s scan.

The 2-hydroxyterephthalic acid (HTA) fluorescence emission of the TA solution with or without US irradiation is shown in Figure 4. TA is a non-fluorescent compound and may further react with hydroxyl radicals to produce a highly fluorescent HTA. The fluorescence was $106 \pm 4\%$ (US group) and $100 \pm 2\%$

(control group), respectively. The fluorescence emission of the control group was 100% as the baseline. Each experiment was repeated 6 times. Based on the result, we believe that the US parameter in this study is able to induce inertial cavitation.

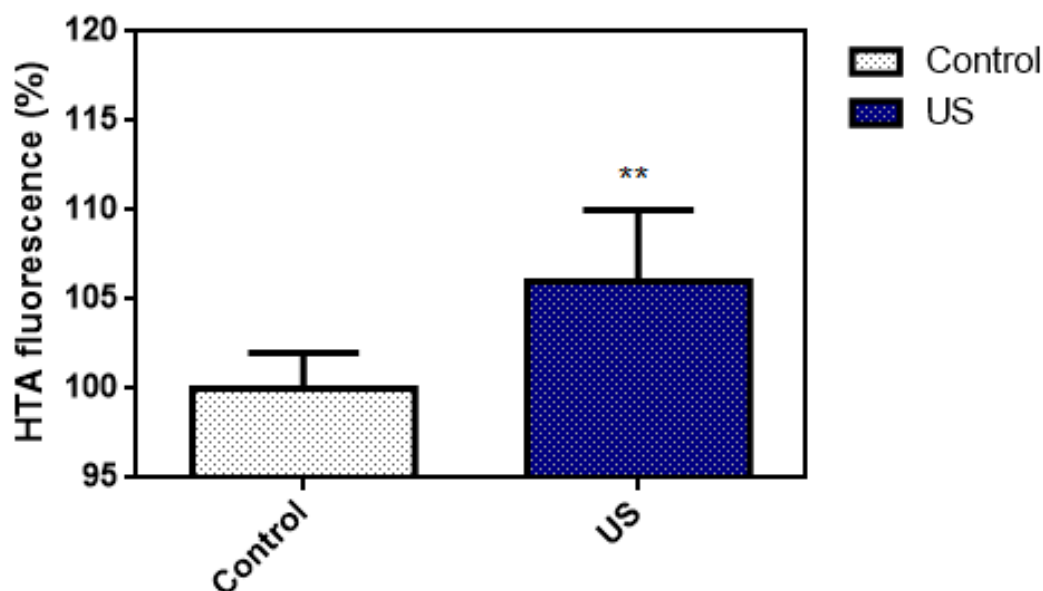


Figure 4. Oxidation of terephthalic acid (TA) to 2-hydroxyterephthalic acid (HTA) in the presence of hydroxyl radicals induced by inertial cavitation (one-way ANOVA, mean \pm SD, $n = 6$, **: $p < 0.01$).

The biocompatibility test of C-doped TiO₂ on cell viability by the WST-1 test is shown in Figure 5. After treatment with C-doped TiO₂, the cell viability was 0.25 \pm 0.24% (positive control group), 99.54 \pm 10% (negative control group), 100 \pm 24% (control group) and 81.49 \pm 20% (C-doped TiO₂ group), respectively. The cell viability of the control group was 100% as the baseline. Each experiment was repeated 5 times. The biocompatibility test followed by the regulations of ISO 10,993 indicated that there would be no potential toxicity when the cell viability of the experiment group was over 75%. Based on the WST-1 test, C-doped TiO₂ showed no potential toxicity to normal cells.

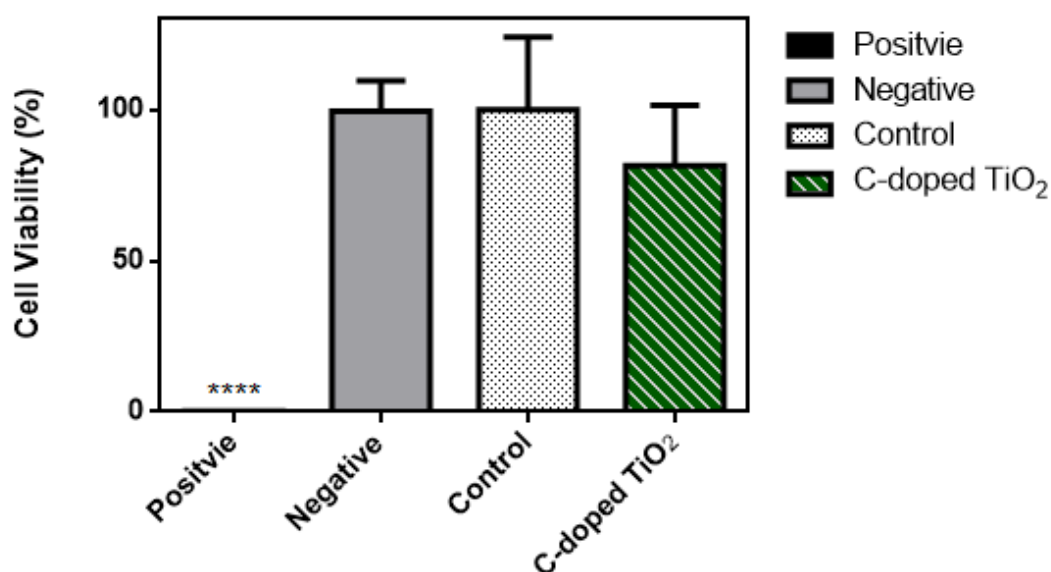


Figure 5. WST-1 test for the biocompatibility of C-doped TiO₂ (one-way ANOVA, mean \pm SD, $n = 5$, ****: $p < 0.0001$).

ROS generation of C-doped TiO₂ under US irradiation by the DCFDA test is shown in Figure 6. DCFDA was able to permeate into 4T1 cells and be deacetylated by cellular esterases to a non-fluorescent DCFH. DCFH was then oxidized to a highly fluorescent 2', 7'-dichlorofluorescein (DCF) in the presence of ROS. After the treatments, the fluorescence was 100 ± 7% (control group), 97 ± 12% (C-doped TiO₂ group), 119 ± 13% (US group) and 141 ± 11% (SDT group), respectively. The fluorescence of the control group was 100% as the baseline. Each experiment was repeated 6 times.

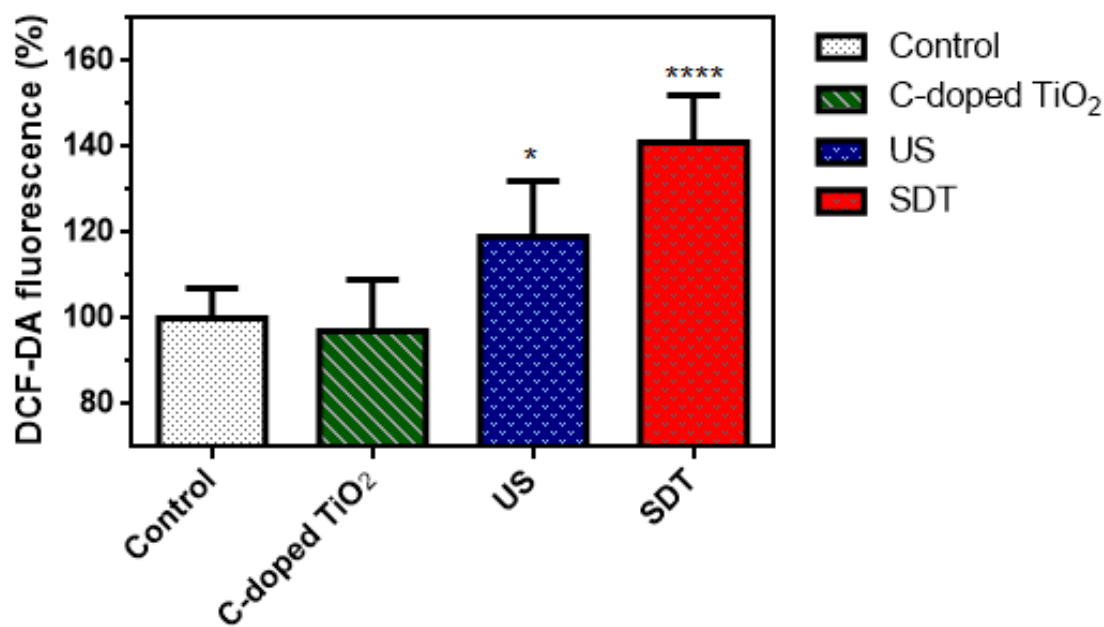


Figure 6. DCFDA test for relative ROS concentration induced by C-doped TiO₂ activated by US (one-way ANOVA, mean ± SD, $n = 6$, *: $p < 0.05$, ****: $p < 0.0001$).

The effect of C-doped TiO₂ in SDT on cell viability and cytotoxicity of 4T1 cells was examined by WST-1 and LDH tests. The results of live/dead assay are shown in Figure S1 to evaluate cell viability in C-doped TiO₂ during ultrasound irradiation. After the treatments, the cell viability was 0 ± 1% (positive control group), 90 ± 13% (negative control group), 100 ± 14% (control group), 84 ± 3% (C-doped TiO₂ group), 77 ± 2% (US group) and 67 ± 7% (SDT group), respectively, as shown in Figure 7a. The cell viability of the control group was 100% as the baseline. Each experiment was repeated 6 times. After the treatments, the cytotoxicity was 100 ± 18% (total lysis group), 0 ± 3% (C-doped TiO₂ group), 7 ± 13% (US group) and 23 ± 13% (SDT group), respectively, as shown in Figure 7b. The cytotoxicity of the control group was 0% as the baseline.

The antitumor efficacy of C-doped TiO₂ under ultrasound irradiation was evaluated using BALB/c nude mice subcutaneously injected with 4T1 cells, where C-doped TiO₂ particles were delivered into mice during the entire experiment and then treated with ultrasound irradiation twice—on day 0 and day 7 (Figures S2 and S3). The variation of relative tumor volume is shown in Figure 8, which was used to evaluate the antitumor effect of C-doped TiO₂ in SDT for 4T1 cells. At 14 days, the relative tumor volume was 367 ± 176% (control group), 407 ± 73% (C-doped TiO₂ group), 335 ± 82% (US group) and 165 ± 22% (SDT group), respectively. The H&E-stained images of organs are shown in Figure S4. The result showed that the C-doped TiO₂ group and US group could not suppress the growth of the tumor. On the other hand, the SDT group could retard the tumor growth significantly ($p < 0.05$). The histologic staining of the tumor site is shown in Figure 9. H&E-stained tumor tissue images confirmed that SDT enhanced the ability to cause the death of the 4T1 cells compared to the other groups.

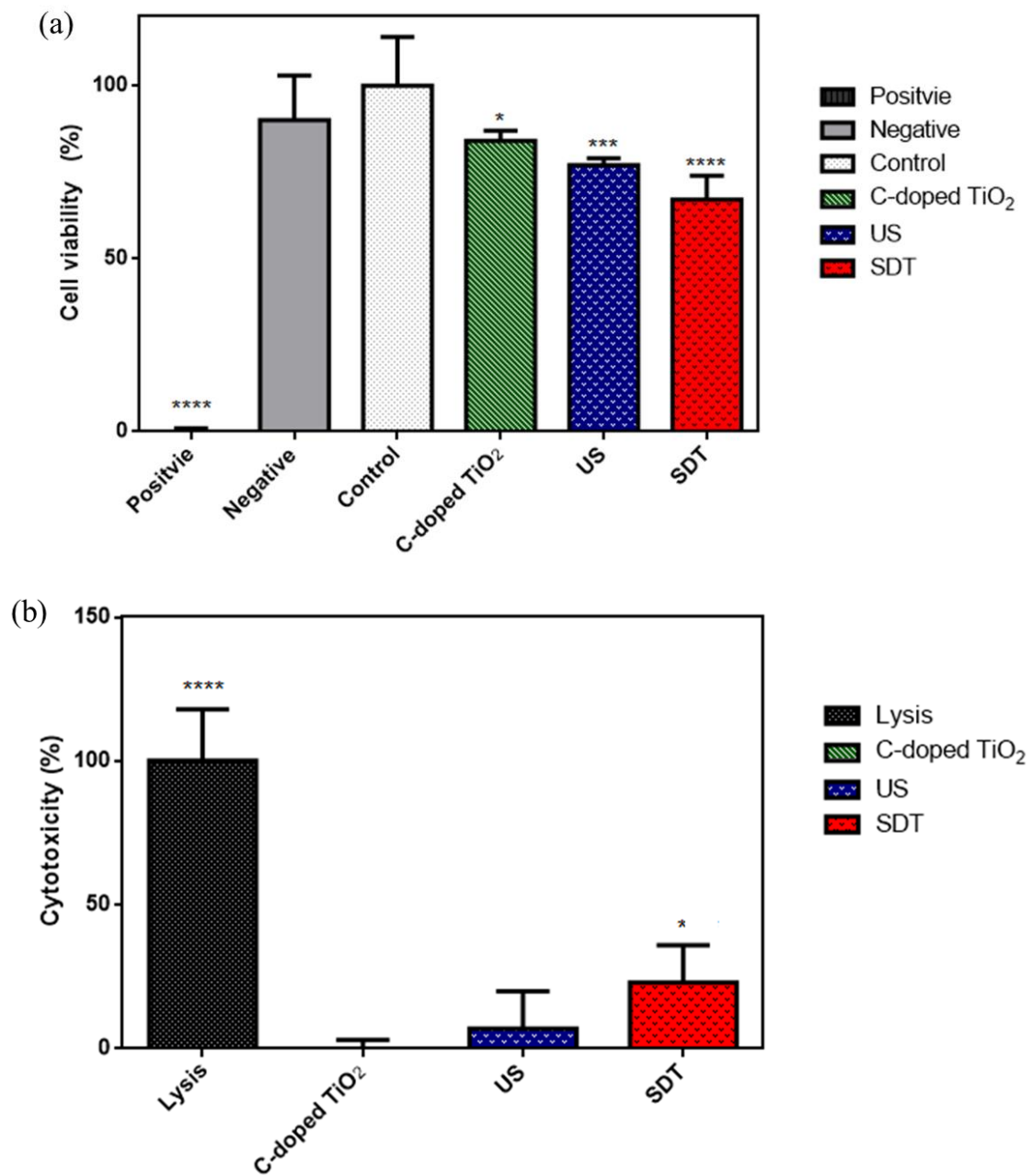


Figure 7. (a) Cell viability induced by C-doped TiO₂ activated by US evaluated by WST-1 assay (one-way ANOVA, mean ± SD, n = 6), (b) cytotoxicity induced by C-doped TiO₂ activated by US evaluated by LDH assay (one-way ANOVA, mean ± SD, n = 6, *: p < 0.05, ***: p < 0.001, ****: p < 0.0001).

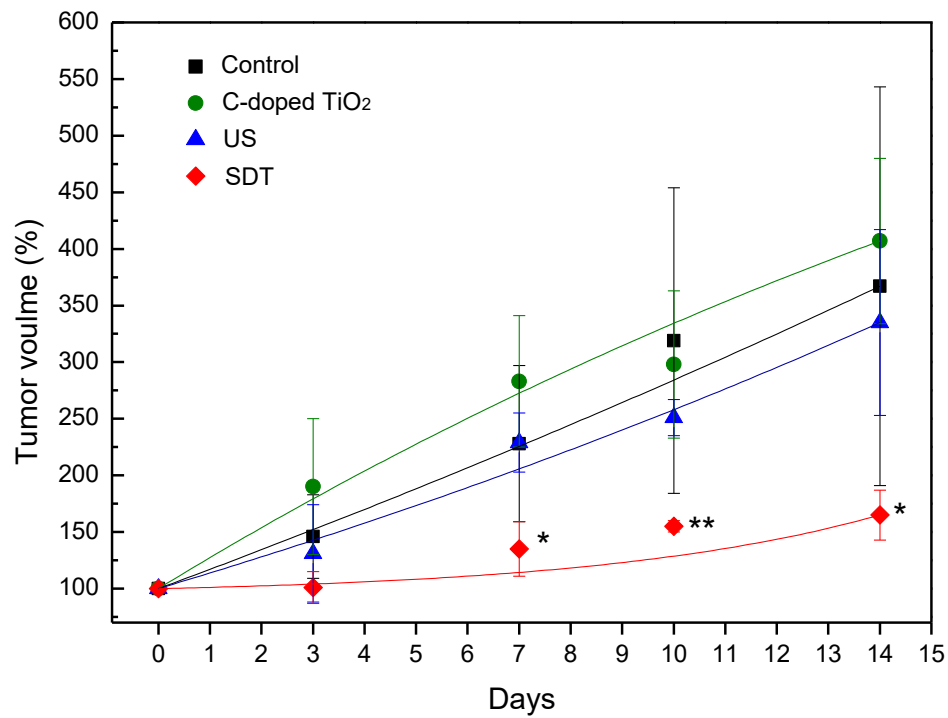


Figure 8. The variation of relative tumor volume in BALB/c nude mice induced by C-doped TiO₂ activated by US (one-way ANOVA, mean \pm SD, $n = 5$, *: $p < 0.05$, **: $p < 0.01$).

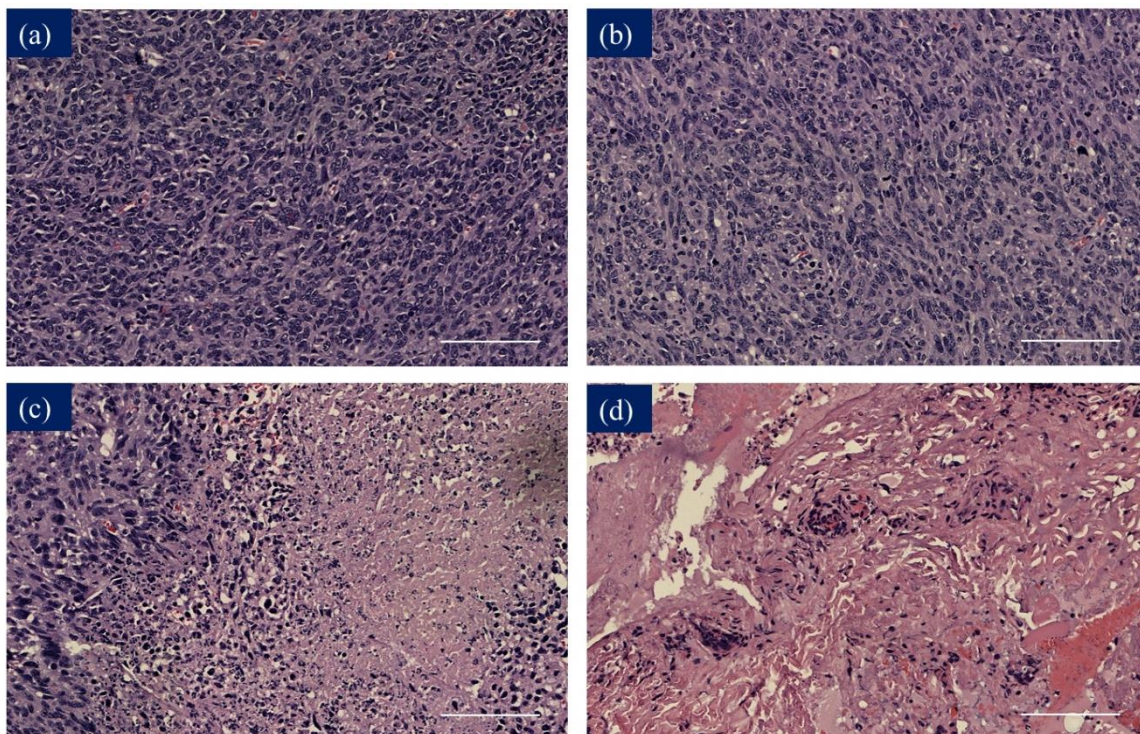


Figure 9. H&E-stained images of tumor tissue. (a) Control group, (b) C-doped TiO₂ group, (c) US group and (d) sonodynamic therapy (SDT) group.

4. Discussion

TiO₂ is one of most representative material studied in inorganic sonosensitizers. Nonetheless, the low quantum yield of ROS limits the effectiveness of TiO₂ as a sonosensitizer by rapid recombination of the free electron and electron hole. The addition of noble metals, such as Pt and Au, have been reported to retard carrier combination [30,31]. Pt-doped or Au-doped TiO₂ has been confirmed to show therapeutic efficacy and suppress the growth of tumors significantly. However, the price of novel metals would increase the cost of material preparation dramatically. Carbon shows highly promising dopant to narrow the bandgap, reaching similar therapeutic efficacy to a novel metal-based system in a more economical way. The comparative table is listed in Table 1.

Table 1. The sonosensitizers and the matched ultrasound parameters.

Tumor/Source	Host	Sonosensitizers	Ultrasound Parameter			Reference
			MHz (f)	W/cm ² (I)	Duration (s)	
Heptaic/human	mouse	TiO ₂	0.5/1.0	0.8/0.4	60	[32]
Skin/mouse	mouse	TiO ₂	1	1.0	120	[33]
Breast/human	mouse	TiO ₂	1	0.1	30	[34]
Lung/mouse	mouse	Au-doped TiO ₂	1.5	30	30	[31]
Breast/human	mouse	Pt-doped TiO ₂	1	1.5	300	[30]

In Figure 2a, the crystal structure of synthesized C-doped TiO₂ was matched with the standard pattern of the anatase structure without significant structure change when carbon atoms played the substitutional foreign atoms, replacing some of the oxygen atoms. The results corresponded with the previous study [35]. In Figure 3c, the peak at around 282 eV was ascribed to Ti-C bonds. Thus, the Kröger–Vink notation of possible substitution of O²⁻ by C was proposed and shown in Equation (2). The creation of oxygen vacancies may form the impurity band that contributes a band tailing effect, thus diminishing the bandgap [36,37]. In the previous study [38], comparing the typical Ti-O binding energy, the clear blue-shift was shown, which indicated the presence of oxygen vacancy after the reduction.



In Figure 2c,g, the particle size of C-doped TiO₂ was 156.9 nm which made the nanoparticles possible to accumulate in tumor tissue without entering the normal tissue [39].

Mechanical index (MI) was one of the indicators for evaluating the occurrence of the inertial cavitation. MI was calculated using Equation (3), where P_r is the peak-negative acoustic pressure and f_c is the center frequency of the ultrasound transducer. It was shown that 0.3 MPa of the peak-negative acoustic pressure was the least pressure to induce the inertial cavitation in aqueous solution [40]. In Figure 4, under US irradiation, the production of HTA increased significantly compared to the control group. In other words, US irradiation is able to elevate the OH generation in TA solution. Hence, the US parameter in this study was confirmed to be effective to induce the inertial cavitation.

$$\text{MI} = \frac{P}{\sqrt{f_c}} \quad (3)$$

In Figure 6, compared to the control group, 4T1 cells treated with C-doped TiO₂ did not increase the level of ROS; 4T1 cells treated with US could be effective to increase the level of ROS, ascribed to the pyrolysis reaction of the water to produce hydroxyl radicals; 4T1 cells treated with C-doped TiO₂ plus US could increase the most significant level of ROS than the other groups, ascribed to the highly reactive singlet oxygen and hydroxyl radicals. This result corroborated that, under US irradiation, ROS generation could be increased in the presence of C-doped TiO₂. However, the amount of extracellular

generation of ROS may affect the cell toxicity of tumor cells. Figure 7 shows that SDT induced higher toxicity in 4T1 cells than the other three groups. The results show that only US treatment seemed to cause insufficient ability to damage the 4T1 cells with the production of hydroxyl radicals. Nonetheless, US treatment in the presence of C-doped TiO₂ seemed to significantly suppress the proliferation of 4T1 cells. The cellular uptake of C-doped TiO₂ to 4T1 cells was supposed to occur via endocytosis or pinocytosis [41]. The possible pathway of cell damage induced by SDT may be speculated as: Under US irradiation, C-doped TiO₂ was activated by the sonoluminescent light, induced by inertial cavitation, to an excited state. Carbon was doped in the anatase TiO₂ to form a new valence band, thus narrowing the bandgap. The addition of carbon may give TiO₂ an excess of conducting electrons or holes, which is important for lowering the bandgap [23,24]. The unstableness of the excited state may cause decay back to the ground state, leading to energy release. The released energy may transfer to oxygen to generate the highly reactive singlet oxygen and water to generate hydroxyl radicals (Figure 10). With the increasing concentration of singlet oxygen and hydroxyl radicals, 4T1 cells would be gradually damaged and lead to cell senescence and death due to oxidative damaging effects [11,42,43]. Due to the enhanced permeability and retention (EPR) effect, C-doped TiO₂ preferentially accumulates in tumor cells eliciting efficient ROS generation [44] and further increasing the effectiveness of the SDT treatment. It was also revealed that the suppression of the tumor is due to the elevated level of ROS which results in both direct tumor cell death and blood vessel stasis. ROS can induce blood stasis via platelet aggregation or vessel constriction by destroying the endothelial layer [45]. Furthermore, SDT may elevate the level of inflammatory-associated cytokine (including TNF-alpha, IL-6, IL-1) production which is known to stimulate the maturation and function of granulocytes and macrophages [46].

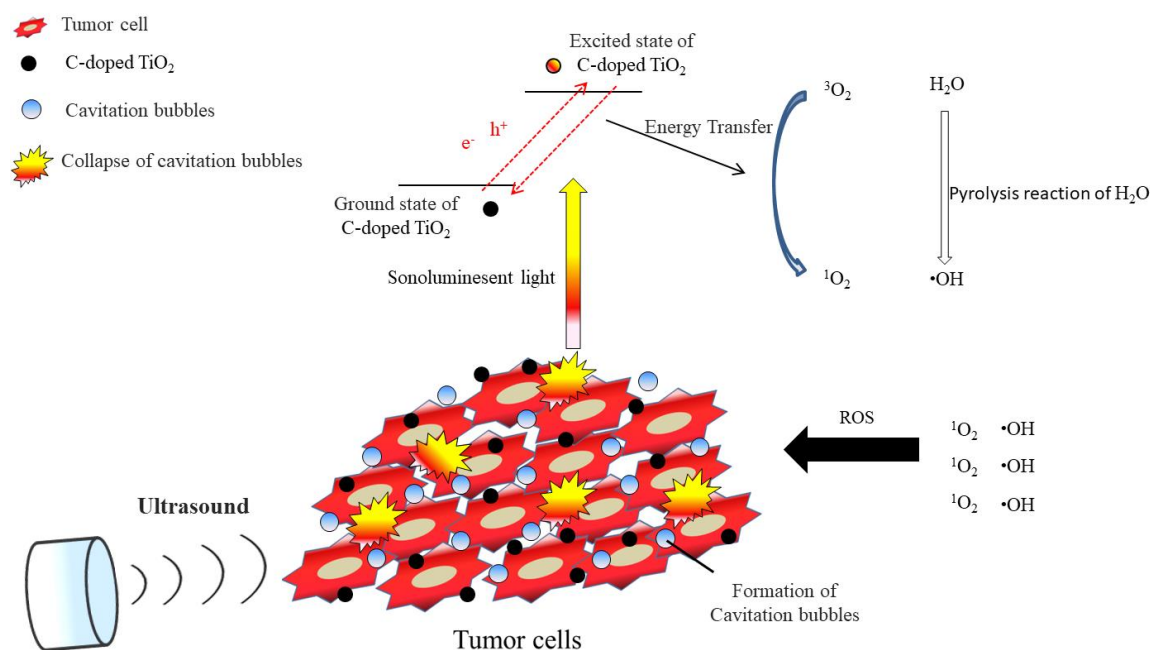


Figure 10. The possible pathway of 4T1 tumor cell damage induced by SDT.

To further investigate the cell death of 4T1 cells induced by SDT, in-vivo study was implemented in this study. Figure 8 shows that SDT could be more effective in suppressing the growth of the 4T1 tumor with a significant difference between SDT and the other groups on day 7. The relative tumor volume of SDT ended with almost half compared to the other groups at the 14th day of the treatment. H&E-stained tumor tissue is shown in Figure 9. In the tumors treated with 1× PBS or C-doped TiO₂ individually, integral tumor cellularity with spindle shape nuclei was visible. In the tumors treated with US, attributed to the inertial cavitation effect of US, a small area of nuclear fragmentation with little necrosis was visible. However, in the tumors treated with SDT, with the synergistic effect of hydroxyl

radicals and singlet oxygen, a huge necrotic area with shrinkage and fragments of nuclei was seen. These results corroborated that SDT could inhibit the proliferation of 4T1 tumor cells.

5. Conclusions

The availability of C-doped TiO₂ nanoparticles as sonosensitizers activated by low-intensity ultrasound to generate ROS for cancer treatment was investigated in this study. Spherical C-doped TiO₂ nanoparticles with an average particle size of around 157 nm were synthesized by the sol-gel process. From the WST-1 test, C-doped TiO₂ showed no potential toxicity to normal cells. From in vitro study, it showed more extracellular generation of ROS in 4T1 breast cancer cells under SDT (C-doped TiO₂/US treatment). Moreover, the effect of C-doped TiO₂ in SDT could reduce the cell viability and increase the cytotoxicity of 4T1 cells. From in vivo study, the antitumor effect of C-doped TiO₂ in SDT may inhibit the proliferation of the 4T1 tumor and lead to a huge necrotic area with shrinkage and fragments of nuclei in the tumor site. We believe that C-doped TiO₂ nanoparticles could be viewed as sonosensitizers in SDT activated by low-intensity ultrasound for ROS generation as an effective strategy for alternative cancer treatments in the future.

Supplementary Materials: The following are available online at <http://www.mdpi.com/2076-3921/9/9/880/s1>, Figure S1: Live/Dead assay; Figure S2: survival rate of BALB/c nude mice; Figure S3: average weight of BALB/c nude mice; Figure S4: H&E-stained images of organs.

Author Contributions: Conceptualization, C.-C.Y. and F.-H.L.; methodology, G.-S.C. and C.-H.H.; software, C.-X.W.; validation, C.-Y.K., C.-Y.C. (Chih-Ying Chi), C.-Y.C. (Ching-Yun Chen) and Y.-Y.L.; formal analysis, C.-X.W.; investigation, C.-Y.K., C.-Y.C. (Chih-Ying Chi), C.-Y.C. (Ching-Yun Chen) and Y.-Y.L.; resources, C.-H.H. and F.-H.L.; data curation, C.-C.Y.; writing—original draft preparation, C.-X.W.; writing—review and editing, C.-C.Y.; visualization, C.-X.W.; supervision, C.-H.H., G.-S.C., and F.-H.L.; project administration, F.-H.L. All authors have read and agreed to the published version of the manuscript.

Funding: This research received no external funding.

Conflicts of Interest: The authors declare no conflict of interest.

References

1. Siegel, R.L.; Miller, K.D.; Jemal, A. Cancer statistics, 2019. *CA Cancer J. Clin.* **2019**, *69*, 7–34. [[CrossRef](#)] [[PubMed](#)]
2. Yang, C.-C.; Wang, W.-Y.; Lin, F.-H.; Hou, C.-H. Rare-Earth-Doped Calcium Carbonate Exposed to X-ray Irradiation to Induce Reactive Oxygen Species for Tumor Treatment. *Int. J. Mol. Sci.* **2019**, *20*, 1148. [[CrossRef](#)] [[PubMed](#)]
3. Yang, C.-C.; Tsai, M.-H.; Li, K.-Y.; Hou, C.-H.; Lin, F.-H. Carbon-Doped TiO₂ Activated by X-Ray Irradiation for the Generation of Reactive Oxygen Species to Enhance Photodynamic Therapy in Tumor Treatment. *Int. J. Mol. Sci.* **2019**, *20*, 2072. [[CrossRef](#)] [[PubMed](#)]
4. Yang, C.-C.; Sun, Y.-J.; Chung, P.-H.; Chen, W.-Y.; Swieszkowski, W.; Tian, W.; Lin, F.-H. Development of Ce-doped TiO₂ activated by X-ray irradiation for alternative cancer treatment. *Ceram. Int.* **2017**, *43*, 12675–12683. [[CrossRef](#)]
5. Umemura, S.; Yumita, N.; Nishigaki, R.; Umemura, K. Mechanism of cell damage by ultrasound in combination with hematoporphyrin. *Jpn. J. Cancer Res. Gann* **1990**, *81*, 962–966. [[CrossRef](#)]
6. Serpe, L.; Foglietta, F.; Canaparo, R. Nanosonotechnology: The next challenge in cancer sonodynamic therapy. *Nanotechnol. Rev.* **2012**, *1*. [[CrossRef](#)]
7. Shibaguchi, H.; Tsuru, H.; Kuroki, M.; Kuroki, M. Sonodynamic cancer therapy: A non-invasive and repeatable approach using low-intensity ultrasound with a sonosensitizer. *Anticancer Res.* **2011**, *31*, 2425–2430.
8. Wood, A.K.; Sehgal, C.M. A review of low-intensity ultrasound for cancer therapy. *Ultrasound Med. Biol.* **2015**, *41*, 905–928. [[CrossRef](#)] [[PubMed](#)]
9. Rosenthal, I.; Sostaric, J.Z.; Riesz, P. Sonodynamic therapy—a review of the synergistic effects of drugs and ultrasound. *Ultrasound. Sonochem.* **2004**, *11*, 349–363. [[CrossRef](#)]
10. Qian, X.; Zheng, Y.; Chen, Y. Micro/Nanoparticle-Augmented Sonodynamic Therapy (SDT): Breaking the Depth Shallow of Photoactivation. *Adv. Mater.* **2016**, *28*, 8097–8129. [[CrossRef](#)]

11. Zou, Z.; Chang, H.; Li, H.; Wang, S. Induction of reactive oxygen species: An emerging approach for cancer therapy. *Apoptosis* **2017**, *22*, 1321–1335. [[CrossRef](#)]
12. Sadanala, K.C.; Chaturvedi, P.K.; Seo, Y.M.; Kim, J.M.; Jo, Y.S.; Lee, Y.K.; Ahn, W.S. Sono-photodynamic combination therapy: A review on sensitizers. *Anticancer Res.* **2014**, *34*, 4657–4664. [[PubMed](#)]
13. Serpe, L.; Giuntini, F. Sonodynamic antimicrobial chemotherapy: First steps towards a sound approach for microbe inactivation. *J. Photochem. Photobiol. B* **2015**, *150*, 44–49. [[CrossRef](#)] [[PubMed](#)]
14. Ninomiya, K.; Ogino, C.; Oshima, S.; Sonoke, S.; Kuroda, S.; Shimizu, N. Targeted sonodynamic therapy using protein-modified TiO₂ nanoparticles. *Ultrason. Sonochem.* **2012**, *19*, 607–614. [[CrossRef](#)] [[PubMed](#)]
15. Zhu, W.; Alkhalil, M.; Cho, M.; Xiao, S. Microbubble generation by piezotransducer for biological studies. *Rev. Sci. Instrum.* **2015**, *86*, 124901. [[CrossRef](#)] [[PubMed](#)]
16. Bhangu, S.K.; Ashokkumar, M. Theory of Sonochemistry. *Top. Curr. Chem.* **2016**, *374*, 56. [[CrossRef](#)]
17. McHale, A.P.; Callan, J.F.; Nomikou, N.; Fowley, C.; Callan, B. Sonodynamic therapy: Concept, mechanism and application to cancer treatment. In *Advances in Experimental Medicine and Biology*; Springer: Cham, Switzerland, 2016; Volume 880, pp. 429–450.
18. Paliwal, S.; Mitragotri, S. Ultrasound-induced cavitation: Applications in drug and gene delivery. *Expert Opin. Drug Deliv.* **2006**, *3*, 713–726. [[CrossRef](#)]
19. Khataee, A.; Kayan, B.; Gholami, P.; Kalderis, D.; Akay, S. Sonocatalytic degradation of an anthraquinone dye using TiO₂-biochar nanocomposite. *Ultrason Sonochem.* **2017**, *39*, 120–128. [[CrossRef](#)]
20. Wan, G.Y.; Liu, Y.; Chen, B.W.; Liu, Y.Y.; Wang, Y.S.; Zhang, N. Recent advances of sonodynamic therapy in cancer treatment. *Cancer Biol. Med.* **2016**, *13*, 325–338. [[CrossRef](#)]
21. Xu, H.; Zhang, X.; Han, R.; Yang, P.; Ma, H.; Song, Y.; Lu, Z.; Yin, W.; Wu, X.; Wang, H. Nanoparticles in sonodynamic therapy: State of the art review. *RSC Adv.* **2016**, *6*, 50697–50705. [[CrossRef](#)]
22. Tong, H.; Enomoto, N.; Inada, M.; Tanaka, Y.; Hojo, J. Synthesis of mesoporous TiO₂ spheres and aggregates by sol-gel method for dye-sensitized solar cells. *Mater. Lett.* **2015**, *141*, 259–262. [[CrossRef](#)]
23. Lin, Y.-T.; Weng, C.-H.; Lin, Y.-H.; Shiesh, C.-C.; Chen, F.-Y. Effect of C content and calcination temperature on the photocatalytic activity of C-doped TiO₂ catalyst. *Sep. Purif. Technol.* **2013**, *116*, 114–123. [[CrossRef](#)]
24. Palanivelu, K.; Im, J.-S.; Lee, Y.-S. Carbon Doping of TiO₂ for Visible Light Photo Catalysis—A review. *Carbon Lett.* **2007**, *8*, 214–224. [[CrossRef](#)]
25. Friehs, E.; AlSalka, Y.; Jonczyk, R.; Lavrentieva, A.; Jochums, A.; Walter, J.-G.; Stahl, F.; Scheper, T.; Bahnemann, D. Toxicity, phototoxicity and biocidal activity of nanoparticles employed in photocatalysis. *J. Photochem. Photobiol. C Photochem. Rev.* **2016**, *29*, 1–28. [[CrossRef](#)]
26. Sazgarnia, A.; Shanei, A. Evaluation of Acoustic Cavitation in Terephthalic Acid Solutions Containing Gold Nanoparticles by the Spectrofluorometry Method. *Int. J. Photoenergy* **2012**, *2012*, 376047. [[CrossRef](#)]
27. Kuan, C.-Y.; Lin, Y.-Y.; Chen, C.-Y.; Yang, C.-C.; Chi, C.-Y.; Li, C.-H.; Dong, G.-C.; Lin, F.-H. The preparation of oxidized methylcellulose crosslinked by adipic acid dihydrazide loaded with vitamin C for traumatic brain injury. *J. Mater. Chem. B* **2019**, *7*, 4499–4508. [[CrossRef](#)]
28. Tomayko, M.M.; Reynolds, C.P. Determination of subcutaneous tumor size in athymic (nude) mice*. *Cancer Chemother Pharm.* **1989**, *24*, 148–154. [[CrossRef](#)] [[PubMed](#)]
29. Huang, W.H.; Lee, S.; Zhang, L.; Li, G.; Yu, J.C. Effect of Carbon Doping on the Mesoporous Structure of Nanocrystalline Titanium Dioxide and Its Solar-Light-Driven Photocatalytic Degradation of NO_x. *Langmuir* **2008**, *24*, 3510–3516. [[CrossRef](#)] [[PubMed](#)]
30. Liang, S.; Deng, X.; Xu, G.; Xiao, X.; Wang, M.; Guo, X.; Ma, P.A.; Cheng, Z.; Zhang, D.; Lin, J. A Novel Pt-TiO₂ Heterostructure with Oxygen-Deficient Layer as Bilaterally Enhanced Sonosensitizer for Synergistic Chemo-Sonodynamic Cancer Therapy. *Adv. Funct. Mater.* **2020**, *30*, 1908598. [[CrossRef](#)]
31. Deepagan, V.G.; You, D.G.; Um, W.; Ko, H.; Kwon, S.; Choi, K.Y.; Yi, G.-R.; Lee, J.Y.; Lee, D.S.; Kim, K.; et al. Long-Circulating Au-TiO₂ Nanocomposite as a Sonosensitizer for ROS-Mediated Eradication of Cancer. *Nano Lett.* **2016**, *16*, 6257–6264. [[CrossRef](#)]
32. Ninomiya, K.; Noda, K.; Ogino, C.; Kuroda, S.-I.; Shimizu, N. Enhanced OH radical generation by dual-frequency ultrasound with TiO₂ nanoparticles: Its application to targeted sonodynamic therapy. *Ultrason. Sonochem.* **2014**, *21*, 289–294. [[CrossRef](#)]
33. Harada, Y.; Ogawa, K.; Irie, Y.; Endo, H.; Feril, L.B.; Uemura, T.; Tachibana, K. Ultrasound activation of TiO₂ in melanoma tumors. *J. Control. Release* **2011**, *149*, 190–195. [[CrossRef](#)]

34. Ninomiya, K.; Fukuda, A.; Ogino, C.; Shimizu, N. Targeted sonocatalytic cancer cell injury using avidin-conjugated titanium dioxide nanoparticles. *Ultrason. Sonochem.* **2014**, *21*, 1624–1628. [[CrossRef](#)]
35. Kamisaka, H.; Adachi, T.; Yamashita, K. Theoretical study of the structure and optical properties of carbon-doped rutile and anatase titanium oxides. *J. Chem. Phys.* **2005**, *123*, 084704. [[CrossRef](#)] [[PubMed](#)]
36. Noorimotlagh, Z.; Kazeminezhad, I.; Jaafarzadeh, N.; Ahmadi, M.; Ramezani, Z. Improved performance of immobilized TiO₂ under visible light for the commercial surfactant degradation: Role of carbon doped TiO₂ and anatase/rutile ratio. *Catal. Today* **2020**, *348*, 277–289. [[CrossRef](#)]
37. Saiful Amran, S.N.B.; Wongso, V.; Abdul Halim, N.S.; Husni, M.K.; Sambudi, N.S.; Wirzal, M.D.H. Immobilized carbon-doped TiO₂ in polyamide fibers for the degradation of methylene blue. *J. Asian Ceram. Soc.* **2019**, *7*, 321–330. [[CrossRef](#)]
38. Han, X.; Huang, J.; Jing, X.; Yang, D.; Lin, H.; Wang, Z.; Li, P.; Chen, Y. Oxygen-Deficient Black Titania for Synergistic/Enhanced Sonodynamic and Photoinduced Cancer Therapy at Near Infrared-II Biowindow. *ACS Nano* **2018**, *12*, 4545–4555. [[CrossRef](#)]
39. Zhou, Y.; Kopeček, J. Biological rationale for the design of polymeric anti-cancer nanomedicines. *J. Drug Target.* **2013**, *21*, 1–26. [[CrossRef](#)]
40. Church, C.C. Frequency, pulse length, and the mechanical index. *Acoust. Res. Lett. Online* **2005**, *6*, 162–168. [[CrossRef](#)]
41. Xie, J.; Pan, X.; Wang, M.; Yao, L.; Liang, X.; Ma, J.; Fei, Y.; Wang, P.-N.; Mi, L. Targeting and Photodynamic Killing of Cancer Cell by Nitrogen-Doped Titanium Dioxide Coupled with Folic Acid. *Nanomaterials* **2016**, *6*, 113. [[CrossRef](#)] [[PubMed](#)]
42. Wang, L.; Mao, J.; Zhang, G.-H.; Tu, M.-J. Nano-cerium-element-doped titanium dioxide induces apoptosis of Bel 7402 human hepatoma cells in the presence of visible light. *World J. Gastroenterol. WJG* **2007**, *13*, 4011–4014. [[CrossRef](#)]
43. Li, Y.; Zhou, Q.; Deng, Z.; Pan, M.; Liu, X.; Wu, J.; Yan, F.; Zheng, H. IR-780 Dye as a Sonosensitizer for Sonodynamic Therapy of Breast Tumor. *Sci. Rep.* **2016**, *6*, 25968. [[CrossRef](#)]
44. Hasanzadeh Kafshgari, M.; Goldmann, W.H. Insights into Theranostic Properties of Titanium Dioxide for Nanomedicine. *Nano-Micro Lett.* **2020**, *12*, 22. [[CrossRef](#)]
45. Volanti, C.; Gloire, G.; Vanderplasschen, A.; Jacobs, N.; Habraken, Y.; Piette, J. Downregulation of ICAM-1 and VCAM-1 expression in endothelial cells treated by photodynamic therapy. *Oncogene* **2004**, *23*, 8649–8658. [[CrossRef](#)]
46. Shi, Y.; Liu, C.H.; Roberts, A.I.; Das, J.; Xu, G.; Ren, G.; Zhang, Y.; Zhang, L.; Yuan, Z.R.; Tan, H.S.W.; et al. Granulocyte-macrophage colony-stimulating factor (GM-CSF) and T-cell responses: What we do and don't know. *Cell Res.* **2006**, *16*, 126–133. [[CrossRef](#)]



© 2020 by the authors. Licensee MDPI, Basel, Switzerland. This article is an open access article distributed under the terms and conditions of the Creative Commons Attribution (CC BY) license (<http://creativecommons.org/licenses/by/4.0/>).